New Journal of Physics
The open access journal at the forefront of physics

Deutsche Physikalische Gesellschaft DPG IOP Institute of Physics

PAPER • OPEN ACCESS

Self-assembly of hierarchically ordered structures in DNA nanotube systems

To cite this article: Martin Glaser *et al* 2016 *New J. Phys.* **18** 055001

View the article online for updates and enhancements.

You may also like

- Ecosystem services bundles: challenges and opportunities for implementation and further research
Nada Saidi and Christopher Spray
- A subregion-based survival prediction framework for GBM via multi-sequence MRI space optimization and clustering-based feature bundling and construction
Hao Chen, Yang Liu, Xiaoying Pan et al.
- Combining climate, economic, and social policy builds public support for climate action in the US
Parrish Bergquist, Matto Mildenberger and Leah C Stokes

This content was downloaded from IP address 3.143.244.83 on 24/04/2024 at 11:24

New Journal of Physics
The open access journal at the forefront of physics

Deutsche Physikalische Gesellschaft DPG
IOP Institute of Physics

Published in partnership with: Deutsche Physikalische Gesellschaft and the Institute of Physics

OPEN ACCESS

RECEIVED
11 January 2016

REVISED
24 March 2016

ACCEPTED FOR PUBLICATION
11 April 2016

PUBLISHED
29 April 2016

Original content from this work may be used under the terms of the Creative Commons Attribution 3.0 licence.

Any further distribution of this work must maintain attribution to the author(s) and the title of the work, journal citation and DOI.

PAPER

Self-assembly of hierarchically ordered structures in DNA nanotube systems

Martin Glaser[1,2,3], **Jörg Schnauß**[1,2,3], **Teresa Tschirner**[1,2], **B U Sebastian Schmidt**[1], **Maximilian Moebius-Winkler**[2], **Josef A Käs**[1] **and David M Smith**[2,4]

[1] Faculty of Physics and Earth Sciences, Institute of Experimental Physics I, Leipzig University, Linnéstr. 5, D-04103 Leipzig, Germany
[2] Fraunhofer Institute for Cell Therapy and Immunology IZI, DNA Nanodevices Group, Perlickstraße 1, D-04103 Leipzig, Germany
[3] M G and J S contributed equally to this work.
[4] Author to whom any correspondence should be addressed.

E-mail: martin.glaser@uni-leipzig.de, joerg.schnauss@uni-leipzig.de, teresa.tschirner@izi.fraunhofer.de, sebastian.schmidt@uni-leipzig.de, moebiusmaxim@yahoo.de, jkaes@physik.uni-leipzig.de **and** david.smith@izi.fraunhofer.de

Keywords: self-assembly, DNA, DNA nanotubes, aster, depletion forces, persistence length

Abstract

The self-assembly of molecular and macromolecular building blocks into organized patterns is a complex process found in diverse systems over a wide range of size and time scales. The formation of star- or aster-like configurations, for example, is a common characteristic in solutions of polymers or other molecules containing multi-scaled, hierarchical assembly processes. This is a recurring phenomenon in numerous pattern-forming systems ranging from cellular constructs to solutions of ferromagnetic colloids or synthetic plastics. To date, however, it has not been possible to systematically parameterize structural properties of the constituent components in order to study their influence on assembled states. Here, we circumvent this limitation by using DNA nanotubes with programmable mechanical properties as our basic building blocks. A small set of DNA oligonucleotides can be chosen to hybridize into micron-length DNA nanotubes with a well-defined circumference and stiffness. The self-assembly of these nanotubes to hierarchically ordered structures is driven by depletion forces caused by the presence of polyethylene glycol. This trait allowed us to investigate self-assembly effects while maintaining a complete decoupling of density, self-association or bundling strength, and stiffness of the nanotubes. Our findings show diverse ranges of emerging structures including heterogeneous networks, aster-like structures, and densely bundled needle-like structures, which compare to configurations found in many other systems. These show a strong dependence not only on concentration and bundling strength, but also on the underlying mechanical properties of the nanotubes. Similar network architectures to those caused by depletion forces in the low-density regime are obtained when an alternative hybridization-based bundling mechanism is employed to induce self-assembly in an isotropic network of pre-formed DNA nanotubes. This emphasizes the universal effect inevitable attractive forces in crowded environments have on systems of self-assembling soft matter, which should be considered for macromolecular structures applied in crowded systems such as cells.

1. Introduction

Mechanisms leading to the self-assembly of ordered patterns have been widely observed over the years in numerous scientific disciplines, in systems comprised of different materials, and over a broad range of time and size scales [1]. Examples reach from theoretical simulations at the atomic scale [2] to the aggregation of amphiphilic lamella [3] and the self-assembly of rod-like viruses [4] to the nucleated growth of spherulite phases in melts of polymers such as isotactic polypropylene (iPP) [5]. Furthermore, spatiotemporal pattern-formation driven by out-of-equilibrium processes can lead to highly complex behaviors [6].

© 2016 IOP Publishing Ltd and Deutsche Physikalische Gesellschaft

In particular, solutions of filamentous polymers show a surprising range of self-assembled states on the mesoscopic scale [7–10]. Although the underlying components can be diverse, some self-assembled types of order found in these systems show characteristics highly similar to those found throughout various disciplines. One prominent example is the presence of star-like 'aster' structures, which are found in diverse systems comprised of fundamentally different materials such as inorganic, ferromagnetic colloids [11, 12], commercial plastics like iPP [5] as well as in several distinct systems of biological origin [7–10, 13–15]. From a biophysical point of view, aster formation was commonly attributed to energy-consuming self-organization caused by the activity of molecular motors. They can actively organize rodlike microtubules [9, 15] or semiflexible actin filaments [7, 10] into radially-clustered, star-like configurations. Recent studies, however, show that these structures form also without converting chemical energy into mechanical work [8, 13, 16]. It is rather a general feature of isotropic filamentous solutions driven by self-assembly effects caused by entropy maximization towards an equilibrated system [8, 13].

It is important to carefully differentiate between the terms 'self-organization' and 'self-assembly', which are often used interchangeably or are understood differently in the various disciplines. For the work presented here, we conform to the definitions given by Halley and Winkler, where the main distinction between the two terms is energy dissipation [17, 18]. Self-organization creates order through a permanent energy dissipation while self-assembly refers to a decrease of the free energy of a given system.

In our study, we investigate a self-assembly process driven by depletion forces. These depletion forces are caused by excluded volume effects in crowded environments and induce a grouping of suspended particles in polymeric or colloidal solutions [19]. Thus, this inherent physical principle relies solely on maximization of overall entropy in crowded systems, which may influence active entities such as the internal machinery of cells [20]. For instance, the addition of a crowding or depletion agent such as polyethylene glycol (PEG) can induce suspended, filamentous biopolymers such as actin to become grouped into aligned, bundled structures with different collective mechanical properties than their singular form [21–25]. By further increasing the concentration of the involved components, these depletion forces cause an arrangement of these biopolymers into hierarchically ordered structures such as asters [8, 13]. These recent findings demonstrate that the formation of ordered structures can also be realized in biopolymer solutions without the actively driven rearrangement of constituents in an energy-dissipating, self-organizing process. Instead, the process is dominated by the local interaction between geometrical arrangement and entropy maximization. This indicates that the intrinsic physical properties of the underlying constituents will have a strong influence on the self-assembly process and formation of hierarchically ordered structures. For example, the bending rigidity of a filament determines the nature of its transverse fluctuation modes, each of which contributes to the overall entropy of the system. These are suppressed when a filament is bundled together with other filaments due to, for example, depletion forces. This entropic cost competes against the entropic gain resulting from depletion-induced association, and the balance between the two will shift depending on the stiffness of the constituent filaments. These types of intrinsic physical parameters such as stiffness have not been accessible in previous studies on the emergence of ordered self-assembly in systems such as actin [8, 13], filamentous bacteriophages [4] or tubes of amphiphilic molecules [3], and therefore their importance has not been investigated. Although strikingly similar self-assembled motifs are observed throughout diverse disciplines covering widely dissimilar underlying molecular components [3–5, 8, 13], a unifying picture is still not described. The underlying problem is twofold: many of the critical physical parameters within any given system cannot be systematically varied in a decoupled manner while a rigorous connection between molecularly dissimilar systems is questionable.

Previously, changing the stiffness of the underlying filament could be only accomplished by either switching to an entirely different material (e.g. from semiflexible actin filaments to more rigid microtubules) or introducing other components such as proteins or chemicals. These changes, however, are accompanied by a different set of properties and alter these systems fundamentally. Other recent studies were able to manipulate the average persistence length of artificial peptide-based helical filaments over a range extending from a few nanometers up to approximately 200 nm [26, 27]. However, to date the mechanical properties of the underlying components cannot be tuned over a large range to study their influence on mesoscopic structure formation, which can be resolved by our approach. Structural programmability of composite, biologically-derived molecular motor constructs through DNA molecules has already been used to reversibly self-organize aster structures in an active, energy-dissipating microtubule- and kinesin-based system [28].

One central aim of our study is to investigate the influence of the filaments' stiffness as one distinct parameter on the formation of hierarchically ordered structures. By utilizing DNA nanotubes with programmable diameters as our model filaments, we are able to vary the persistence length, which is a measure of stiffness, without changing the basic material.

Here, we do not rely on naturally occurring components but use synthetic constructs with well-defined and fully tunable properties. These DNA nanotubes are formed by a tile-based design, where partial complementarity between neighboring strands in a cyclical manner lead to enclosed rings of double-helical

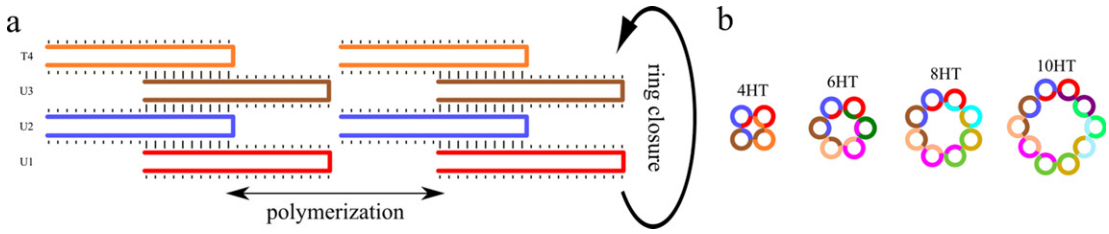

Figure 1. Formation of n-helix tubes. (a) The schematic shows the secondary structure of thin sheets consisting of four, specifically designed DNA oligonucleotide 'tiles' forming a 4-helix tube (4HT). These strands have partially complementary sequences to drive the polymerization of DNA sheets. The set of strands are designed in a cyclical manner, which causes the sheet to close into a ring-like configuration. Due to the staggered design of neighboring tiles, these monomer-like rings can effectively polymerize, leading to a DNA nanotube. This basic design can be extended to form nanotubes with more strands and larger circumference. (b) We employed four different types of nanotubes with differing persistence lengths. As indicated in the cross sections, the strand numbers 4HT, 6HT, 8HT, and 10HT were used in this study. Inspired by [30].

segments with a discrete diameter (figure 1). Due to the staggered arrangement of neighboring tiles, the hybridization of further oligonucleotides leads to the formation, or effective polymerization, of filamentous DNA nanotubes typically measuring several microns in length [29, 30]. A similar DNA-based tube design has in fact been demonstrated to exhibit similar polymerization kinetics as actin filaments and microtubules [31] supporting the applicability of this purely synthetic model system. By varying the number of DNA strands which make up the basic ring structure, the nanotube's architecture as well as its circumference can be controllably varied (figure 1(b)). Slightly changing the circumference leads to a corresponding change in the nanotube's mechanical properties quantified as an altered persistence length [29].

The formation of complex, mesoscopic, condensed aggregates consisting of repeating DNA motifs generated by PCR reactions has been previously addressed, for instance, in the frame of medical applications [32–36]. Other studies have focused on mesoscopic crystallization phases of short, non-hybridizing DNA oligomers through either end-to-end stacking or crowding effects [37–39].

In our study a chosen set of DNA sequences was used to hierarchically assemble large, isolated mesostructures consisting of precisely defined, structurally programmable filamentous subunits. The effect of systematically altering the stiffness of these DNA filament subunits was shown to significantly impact the final self-assembled architecture. We systematically studied a broad range of emerging self-assembled structures within hierarchically defined systems consisting of rodlike or filamentous DNA nanotube subunits.

2. Materials and methods

2.1. DNA nanotube formation

DNA nanotubes were hybridized from single stranded DNA sequences with a length of 42 nucleotides. All sequences (appendix table A1) were purchased from Biomers with HPLC purification. Lyophilized DNA sequences were diluted in double distilled water to a desired concentration. This concentration was measured by absorption spectroscopy at 260 nm using a Nanodrop 1000 (Thermo Fisher Scientific Inc., USA). In order to hybridize a nanotube of a desired strand number n, sequences U1 to U($n-1$) and Tn were mixed in TE buffer (20 mM Tris, pH 7.6, 2 mM EDTA) containing 12.5 mM Mg^{2+}. For fluorescent visualizations of these nanotubes, modified U1 oligonucleotides were used. These strands carried a fluorescent Cyanine dye 3 (Cy3) modification at the 5' end and featured two additional thymine bases in between acting as spacer. U1-Cy3 was added at one fifth of the total desired oligonucleotide concentration for labeling. PEG (35 kDa—Sigma-Aldrich) was used as a crowding agent in different concentrations to induce depletion forces in the system.

For an alternative bundling mechanism without additional depletion agents, the existing sequences have been replaced by modified ones. The two modified strands (U2 and U3) were ordered with an additional shorter sequence separated by three spacer thymine bases. These sequences are complimentary to each other and have been chosen due to their significantly lower melting temperature compared the other matching sequences. This ensures that the bundling occurs after the formation of the nanotubes and does not interfere with their hybridization.

Final sample mixtures were placed between two Sigmacote-passivated glass slides (Sigma-Aldrich) and sealed with vacuum grease and nail polish in order to prevent evaporation.

Within these chambers, the DNA nanotubes were hybridized according to the original protocol by Yin *et al* [30] in a custom-build thermocycler device appropriate for their geometry. The temperature ramp started at 90 °C and was held constant for 10 min before decreasing the temperature to 65 °C over 30 min. The sample was

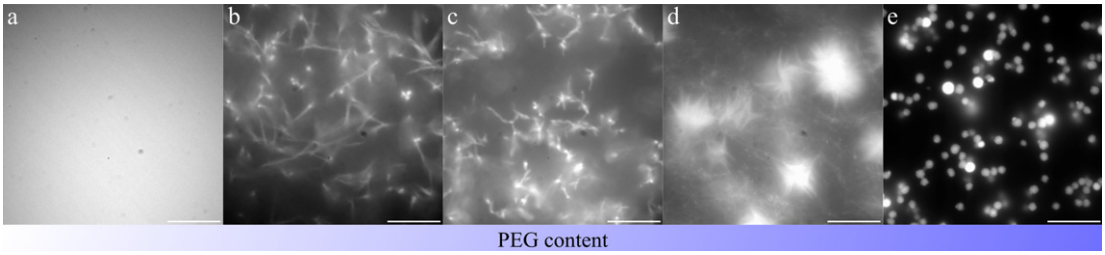

Figure 2. Transition of 32 μM 6HT from an isotropic network to ordered bundles and needle-like structures with increasing PEG content. The PEG content for each sample was: (a) 0%, (b) 2.5%, (c) 5%, (d) 10%, and (e) 15%. The scale bar is 20 μm.

allowed to equilibrate for an additional 30 min and subsequently the temperature was dropped by 0.5 K every 30 min for a total duration of 10 h. After finishing the temperature ramp the setup cooled to room temperature over the course of two hours. During the entire folding process the temperature within the device was monitored with a PT1000 sensor (Heraeus).

2.2. Imaging techniques

Fluorescence measurements were performed using an epi-fluorescence Leica DM IRB microscope equipped with a 100 $\times$ oil-immersion objective (Leica 11506168) and an iXon DV887 back illuminated EMCCD camera (Andor Technology). Fluorescence excitation was induced with a mercury vapor lamp and an N2.1 filter cube (Leica 11513882, excitation filter from 515 to 560 nm) transmitting only the wavelength exciting Cy3 to the sample. Images were recorded as grayscale pictures with the camera-associated Andor SOLIS software.

2.3. Analytical tools

Recorded grayscale images were analyzed using ImageJ and the available plugin *Ridge Detection* (http://fiji.sc/Ridge_Detection). This plugin is based on the detection algorithm described by Steger [40] for detecting ridges and lines. Acquired raw data from this routine yielded the line-width of the detected objects (appendix figure A1). Data was further processed using IPython [41] and MATLAB (the Mathworks, R2013a). Analysis has been performed for all conditions where bundles occurred, either as the exclusive feature, or as a part of a coexistence state with asters or needle-like structures. We excluded small structures from further analysis, which were in fact detected by the algorithm but cannot be treated as a bundle of DNA nanotubes (figure A1(b), white circle). These features can originate, for instance, from other bundles outside of the focal plane or due to the stochastic nature of the assembly process. Thus, small debris with no apparent elongated structure can occur, which cannot be considered as parallel bundles of DNA nanotubes and should not be accounted for determining the line width.

3. Results

3.1. Formation of complex structures depends on depletion strength

The system employed in this study offered a variety of advantages. Since the formation of nanotubes is based on DNA hybridization, the polymerization process from individual strands to elongated nanotubes can be triggered solely by temperature change (section 'DNA nanotube formation'). This allowed us to premix all required ingredients, seal them in a closed system, and then trigger the assembly process by subjecting it to an appropriate temperature ramp. At the origin of the ramp, the high temperature (90 °C) prevents the hybridization of complementary DNA segments of the length used here, ensuring that the single-stranded tiles are in an isotropic state. Having an isotropic closed system in the beginning prevents influences of network history on the outcome. The impact of network history on ordered self-assembly has been reported earlier for other polymeric systems [8, 13]. Depletion forces were introduced using the chemically inert, temperature resistant polymer PEG [19].

Depletion strength was altered via a stepwise increase of PEG content. A representative example is shown in figure 2 for a 6-helix tube (6HT) at a concentration of 32 μM for each type of single-stranded DNA tile (netting roughly 0.25% (w/v) for total DNA content). The network undergoes a clearly visible transition from an isotropic (figure 2(a)) to an anisotropic network already for small amounts of PEG (2.5%, w/v) (figure 2(b)). Characteristic bundles form at low PEG concentrations up to 5% (figure 2(c)). The system then undergoes a sharp transition to larger, more complex structures for high PEG concentrations (10%) (figure 2(d)). These structures display a more radial arrangement, reminiscent of aster morphologies seen in other systems [5, 7, 9, 10, 42]. For higher PEG concentrations at or beyond 15%, depletion forces are so strong that the system is compressed to small condensed aggregates (figure 2(e)). These different PEG regimes have been investigated

for all DNA nanotubes. Since 2.5% PEG and 5% PEG do not show a noticeably different morphology, the 2.5% PEG samples will not be shown later in the text.

3.2. Influence of DNA nanotube stiffness on self-assembled states

To fully investigate the assembly characteristics of DNA nanotubes under the influence of depletion forces, we also varied the characteristics of the tubes themselves. Our approach was two-pronged: the effect of altering the overall nanotube density was determined by scanning through a wide range of DNA tile concentrations, and the influence of mechanical stiffness was analyzed by scanning through PEG and DNA concentrations for each of the four utilized nanotubes with different persistence length. Effectively, this allowed us to independently scan through three decoupled parameters; nanotube density, association strength, and mechanical stiffness.

By using programmable DNA nanotubes the persistence length of the underlying filaments can be controlled by their architectural design [29]. Four different types of nanotubes were investigated in this study: 4-helix tubes (4HT), 6-helix tubes (6HT), 8-helix tubes (8HT), and 10-helix tubes (10HT). Previous studies have revealed a polydisperse length distribution for these nanotubes with a mean length of about 6 μm [30]. Persistence length measurements by Schiffels *et al* [29] for the investigated nanotubes and previously unpublished ones for 4HT have been confirmed by our own measurements for our conditions (data not shown). This allows us to investigate different stiffness regimes. With a persistence length of ~1.2 μm, 4HT resemble a more flexible regime with a ratio of persistence length (l_p) to mean length (L_{mean}) of 0.2 for an individual nanotube. 6HT feature a persistence length of ~3.2 μm and an l_p-to-L_{mean} ratio of 0.5 while 8HT feature a persistence length of ~8.9 μm and an l_p-to-L_{mean} ratio of 1.4. These two tube populations approach what is considered a semiflexible regime. 10HT fall in a stiffer, although not rod-like ($l_p \gg L_{mean}$) regime, with a persistence length of ~12.7 μm and an l_p-to-L_{mean} ratio of 2.1. This set of DNA nanotubes covers one order of magnitude in stiffness without further changes to the chemical or material properties of the system. The change in diameter of the nanotubes leading to the difference in persistence length is on the scale of nanometers, and changes roughly by a factor of two (from approximately 5 nm for 4HT to 9 nm for 10HT) for the entire range of investigated nanotubes. It can be expected that the diameter of individual nanotubes has a minor influence with respect to the comparatively larger change in stiffness.

Typical assembly characteristics of the different types of nanotubes for different concentrations and under varying depletion forces are shown in figure 3. The self-assembled structures are visualized by representative fluorescent images in each image series.

For low DNA concentrations (16 μM) and low PEG content (5%), each of the four investigated types of DNA nanotubes form bundled networks (bottom left panel of each image series). With increasing stiffness, the observed bundles appear shorter and denser. Characteristic aster-like structures, reminiscent of those seen in other systems [8–10, 43], can only be observed using 4HT at these conditions. These structures can be recognized by their radial appearance, with an interconnection point in the center of several merging bundles. For higher PEG content (10%) at low DNA concentrations (upper left panel) the networks changed into an irregular aster-like state, except for 10HT, which still resembled thick short bundles. For 4HT it was possible to increase the PEG content even further to 15% without completely condensing the system. Again isolated aster-like structures could be observed (appendix figure A2). All other DNA concentrations for 4HT and the three other types of nanotubes used showed condensed aggregations at 15% PEG (data not shown).

For intermediate DNA concentrations (32 μM) and low PEG content (bottom middle panel), bundled networks with decreasing length for increasing nanotube stiffness could again be observed for the three stiffer types of nanotubes, while 4HT show aster-like structures which are interconnected via long bundles. This characteristic morphology is conserved for the 4HT when going to high PEG content (top middle panel). In contrast, for the other stiffer nanotubes at 32 μM DNA concentration and high PEG content a new type of characteristic structure emerges. Due to their highly similar morphology to structures reported for the assembly of amphiphilic building blocks by Losensky *et al* [3], we likewise adopt their naming convention of 'needle-like structures'. These large structures are fundamentally different in their appearance. They are significantly more compact, without showing long outgrowths of thin bundles as seen in the aster-like structures, and are on the scale of several tens of micrometers. While the softer 6HT show a coexistence of an intertwined bundled network with needle-like structures in-between, 8HT and 10HT show only the needle-like state for these conditions. This needle-like state was not observed for 4HT under any of the tested conditions.

For higher concentrations, there was a practical limitation on the larger-diameter nanotubes. Inherent errors in accurately pipetting small volumes of highly viscous concentrated PEG solutions together with increasingly large sets of highly concentrated (1 mM and higher) DNA oligonucleotide tiles would require, for example, lyophilization of DNA tile sets. Therefore, in order to maintain consistency in sample preparation across all regimes, a slightly lower maximum DNA concentration for 10HT (50 μM) was used compared to the other types of nanotubes (64, 80 μM). For 4HT the highest DNA concentration (80 μM) at low PEG content did

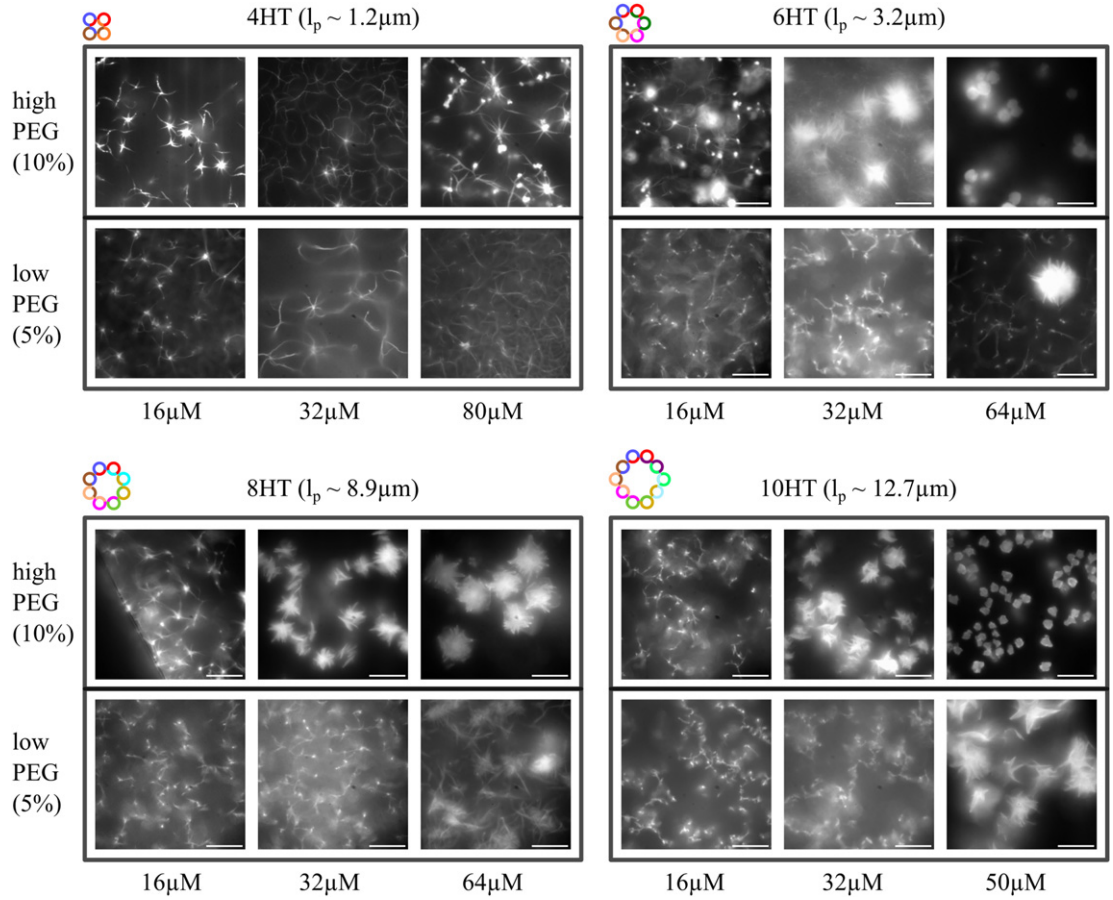

Figure 3. Observed self-assembled state for all investigated DNA nanotubes for low (5%) and high (10%) PEG content. The concentration written below the panels represents the concentration of each DNA oligonucleotide tile and thus of the nanotube unit-rings. Scale bar is 20 μm. A more detailed representation can be found in figure A3 (appendix).

not show characteristic aster-like structures as observed before (bottom right panel), but rather an isotropic network of bundles. This might be attributed to the increasing steric hindrance exerted between the formed bundles, which limits the possibility for them to arrange into centralized aster clusters. For higher PEG content (upper right panel) isolated asters still appeared for the 4HT. For the stiffer nanotubes (6HT, 8HT, and 10HT) a state involving needle-like structures could already be observed for low PEG content (bottom right panel). In the case of 6HT and 8HT, a coexistence of needle-like structures embedded in a bundled network similar to that seen at lower DNA concentrations was observed. For the stiffer 10HT, even though the maximum concentration of 50 μM is somewhat lower than for the 6HT and 8HT, a full transition to exclusively needle-like structures with no evidence of a remaining background network of bundles was clearly evident. For these higher DNA concentrations, only condensed aggregates occurred for 6HT and 10HT with higher PEG content (upper right panel). In contrast, 8HT still formed large, isolated needle-like structures under these conditions. In the absence of PEG all samples showed isotropic networks comparable to figure 2(a) (data not shown). Birefringence measurements did not reveal any nematic alignment or characteristic zebra stripe patterns previously reported in highly concentrated solutions of semiflexible filamentous biopolymers [44].

3.3. The relation of assembly behavior to the thickness of DNA nanotube bundles

A deeper insight into the behavior of the involved bundled structures is given in figure 4. Samples have been analyzed and evaluated as described in section 'analytical tools'. Here, we monitored the line-width thickness of DNA nanotube bundles in all low-PEG (5% PEG) samples where they appeared. This included states consisting solely of bundle or aster-like structures, as well as the coexistence states where bundles appeared together with aster- or needle-like structures. Samples exhibiting only needle-like structures or condensed aggregates were not suitable for evaluation here. This measure of line-width should not be mistaken for an absolute bundle thickness due to the fluorescent labeling; instead it allows a way to compare influence on the basic bundling mechanism at different conditions. We expect that there is a roughly direct correlation between the detected line width and the thickness of the bundle beyond a minimum threshold defined by the diffraction limit. Resultantly, any increases

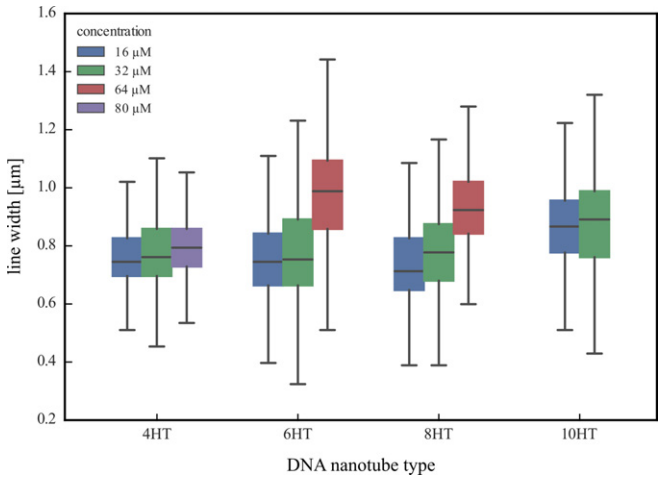

Figure 4. Boxplot for width distributions of bundled structures appearing in all relevant states for each of the utilized DNA nanotubes in low-PEG (5%) conditions. The back line represents the median, the surrounding colored box includes 50% of all data, and the whiskers all data within the 1.5 interquartile range. Analysis has been performed for all conditions where bundles occurred, either as the exclusive feature, or as a part of a coexistence state with asters or needle-like structures.

in the bundle thickness will lead to a monotonic increase in the observed line width. However, there is no current method to reasonably determine this proportionality factor and thus the number of involved filaments.

The observed bundle line-width thickness is comparable for all different types of nanotubes and concentrations in the system within constraints provided by the resolution limit of our setup (figure 4), displaying values between approximately 700 nm and 1 μm. This is consistent for all four types of nanotubes used, as well as across the broad range of DNA tile concentration range from 16 to 80 μM. For both 6HT and 8HT, a non-negligible increase of approximately 20%–30% in bundle thickness is evident for the highest (64 μM) concentrations of DNA tiles where a coexistence with needle-like structures was observed, as compared to the respective bundle-only state for the same nanotube diameter.

3.4. Alternative bundling mechanism

We implemented an alternative attractive binding mechanism between DNA nanotubes based on the hybridization of complementary, single-stranded DNA segments connecting the assembled nanotubes. For this, two of the usual DNA oligonucleotide tiles were appended with an additional sequence at the 5′ end (section 'DNA nanotube formation'). These sequences were complementary to each other in order to enable binding. They were situated far enough apart on the tube surface to ensure that only binding between different nanotubes was possible, and the melting temperature of the complementary segments was chosen to be low enough to ensure that these connections formed at a later time point in the temperature ramp than where the nanotubes themselves are formed. This enabled an investigation of whether, in principle, bundled structures could be also formed starting from an isotropic network of pre-assembled DNA nanotubes where the bundling force is selectively 'switched on', as opposed to via depletion forces which are also present during the formation of the nanotubes themselves.

The most drastic effect has been observed for 4HT (figure 5(a)). At 16 μM DNA concentration, even in the complete absence of any other component such as PEG, they form a clearly inhomogeneous network of bundled structures as a result of the hybridization-based connection of neighboring nanotubes. These are similar in appearance to low-PEG, low-DNA concentration samples for stiffer 6HT (figure 3), and can be clearly distinguished from the usually occurring isotropic networks at 0% PEG (figure 2(a)). Curiously, further increasing the DNA concentration weakens the bundling effect, so that it becomes dominated by large, unbundled, isotropic domains (figure 5(b)). This behavior is in direct opposition to our earlier observations that an increase in concentration leads to the appearance or domination of more compact structures, and might be attributed to the increasing steric hindrance for denser networks as will be addressed later in the discussion.

4. Discussion

In this study we present a highly diverse range of emerging structures induced by a local attractive force acting on DNA nanotubes in solution.

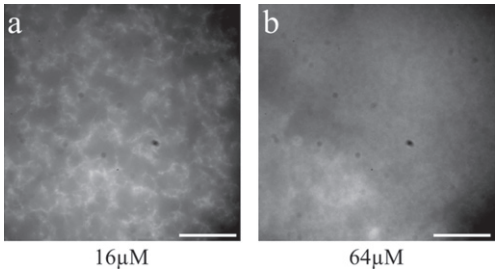

Figure 5. Emerging bundling and density fluctuations due to the alternative bundling mechanism. 4HT carried additional complementary DNA segments and were measured for (a) low and (b) high concentrations. The scale bar is 20 μm.

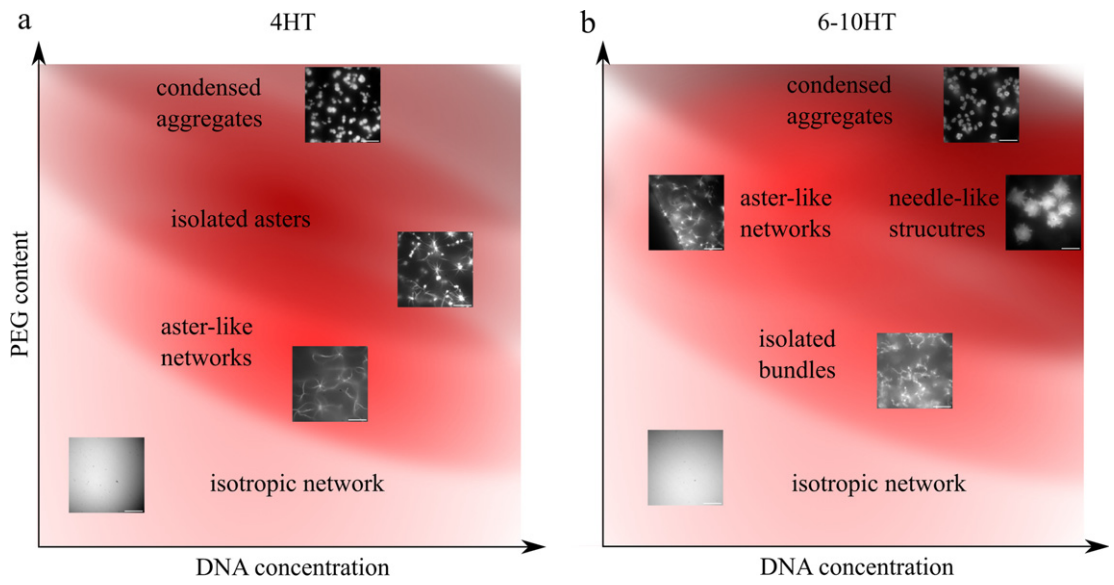

Figure 6. Suggested diagram for observed self-assembled states, as a function of the attraction strength (depletion forces) and DNA concentration. (a) Flexible nanotubes (4HT). (b) Semiflexible and stiffer nanotubes (6–10HT).

The architecture of self-assembled structures was found to depend on the strength of the induced attraction, the concentration of the underlying DNA nanotubes as well as their mechanical properties. For the first time, we investigated the influence of these mechanical properties in a manner entirely decoupled from the other parameters, by altering nanotubes' architectural design to controllably vary their persistence length. Through this, we give a broader view of the interaction and self-assembly of filamentous, rod-like polymers within a crowded environment without any necessity to change our basic material.

Having this unique possibility to cover one decade of persistence length in addition to scanning a wide range of both DNA and PEG concentrations, we were able to generate a broad range of structures. These are highly reminiscent to those that have been observed in systems with vastly different types of constituent materials [3, 7, 8, 10, 39, 43], although in our case occurring within a single material system. We could confirm and further generalize that association of filaments in solutions into hierarchically ordered structures is a general feature of unspecific, attractive interactions between filaments starting from an isotropic initial state. Structures occurred by mere energy minimization and entropy maximization of the system, towards an equilibrium state, without the need to actively dissipate energy. We see a clear impact of the underlying architecture of the component DNA nanotubes on the final assembled state. A graphical representation of this complex behavior is summarized in an approximate diagram suggested in figure 6. We note that this overview aims to combine the diverse regimes and drawn boundaries are only chosen to guide the eye. Transitions from one regime to another cannot be resolved with the used closed systems since initial starting conditions cannot be altered within one sample.

More flexible 4HT characteristically form long interconnected bundles with star- or aster-like arrangements for PEG concentrations above a minimum threshold (figure 6(a)). Even for very high PEG concentrations (>15% PEG) they were able to form asters at lower DNA concentrations (16 μM), although they did exhibit condensed aggregated states at high DNA concentrations. The emergence of the dense, although still highly

ordered needle-like structures was never evident for 4HT under any conditions. This is in stark contrast to the observed behavior typical for the stiffer 6HT, 8HT, and 10HT (figure 6(b)). These displayed a far richer variation in self-assembled morphologies, including bundled networks, aster-like structures and the dense needle-like structures, as well as evidence of coexistence states of aster or needle-like structures embedded in a bundled network. The general trend here was that a shift towards either higher DNA or PEG concentration, i.e., a higher component density or increase in attractive depletion forces, led to the preferred formation of the needle-like structures. For these stiffer filaments, the effect of varying the underlying nanotube stiffness is less clear. As evidenced by the behavior observed in 10HT, the onset of denser morphologies like the needle-like structures or condense aggregates is shifted to lower DNA concentrations (figure 3). This is suggested by the appearance of completely isolated needle-like structures already at a DNA concentration of 50 μM for the 10HT, whereas the significantly higher concentration of 64 μM for 6HT and 8HT still shows a coexistence with bundles.

A detailed analysis of the thickness of the bundled structures appearing in the different states (excluding those exhibiting purely needle-like or condense aggregate structures) showed evidence of a maximum limit on the numbers of filaments, or simply the amount of DNA, which could be associated longitudinally into a bundle (figure 4). A consistent value ranging from 700 nm to 1 μm for the line-width of bundles in fluorescence images was seen over a broad range of total DNA concentration for all four types of tubes, with a noticeable jump of 20%–30% for bundles measured in a coexistence state with needle-like structures.

The similar bundle thickness appearing over both a two-fold variation in nanotube diameter as well as a five-fold variation in concentration is consistent with previous observations on other filamentous systems that suggested an effective upper limit in the number of filaments that can be added to a bundle formed by depletion forces [24]. This is likely due to the fact that material-specific effects such as surface charge repulsion between negatively charged DNA nanotubes must be balanced with depletion-induced attraction. Such a balance could be expected to eventually limit the addition of more filaments to a bundle, even with large increases of material available to contribute to bundles (e.g. the five-fold increase of total DNA content for 4HT).

The aforementioned jump in average bundle thickness emerging in the co-existence states with needle-like structures in 6HT and 8HT could be evidence of a change in the assembly process of the underlying components. This could happen due to an increasing tendency for repeated, lateral growth of the DNA structures perpendicular to what would be considered the tube axis, resulting in the formation of extended sheet-like architectures rather than discrete tubes. While earlier studies on this type of DNA nanotube design have clearly shown that discrete tubes are preferred for the lower concentrations up to approximately 3 μM per tile [30], the drastically higher amounts used here in combination with local concentration enhancement of growing filaments due to depletion forces could be responsible for affecting the assembly process of the constituent DNA structures themselves. This can ultimately lead to a shift to states containing the observed needle-like structures. Curiously, the structurally similar, needle-like 'rosettes' consisting of amphiphilic molecules as previously reported by Losensky *et al* do originate from giant unilamellar vesicles, which are effectively a single sheet in a spherical geometry [3].

Employing an alternative, hybridization-based bundling mechanism, which was triggered after an isotropic network of fully-formed DNA nanotubes hybridized, showed that we could recreate density fluctuations and bundling in our system comparable to low PEG concentrations (figure 5). However, for higher DNA concentration, this effect weakened possibly as a result of steric hindrance causing decreased mobility of nanotubes. Without the possibility for individual nanotubes to rearrange, they are caught in a frustrated state. It has been previously reported that drastically decreased mobility suppresses self-assembly and the formation of patterns [1]. While this hybridization-based bundling mechanism offers a number of tunable parameters pertaining specifically to the bundling mechanism and merits its own in-depth study, this simple demonstration gives indication that the direct coupling of DNA nanotube growth together with the simultaneous bundling resulting from depletion forces might be crucial for the assembly of more complex and dense structures, particularly at higher densities.

This apparent congestion at higher densities is evidence that the concomitant assembly and bundling of nanotubes in samples dominated by depletion forces are important for assembly. This suggests an assembly mechanism driven by the radial outgrowth of semi-rigid polymerizing DNA nanotubes from nucleation points formed by depletion-induced aggregation of initially hybridized segments consisting of a few oligonucleotides. Once these growing, hybridized segments become large enough in comparison to the PEG molecules, they will be subject to depletion forces and bundling to other segments. The addition of new tube segments to a growing nucleus enhances its spatial area, or collision cross-section available for the bundling with further radially growing DNA nanotubes. This type of mechanism has been suggested as an explanation for the observed growth of aster-like structures in actin-myosin solutions undergoing the transition from an actively dissipative to passive crosslink-dominated state [10].

In our study we demonstrated how the hierarchical combination of specific (DNA hybridization) and non-specific (attractive potential) self-assembly leads to a broad variety of complex structures. Here, the rigidity of

well-defined DNA-based nanotubes is observed to be a key parameter in the final morphology of the assembled state, in addition to the density and attractive force between the filamentous components. The assembled architectures not only bear a strong resemblance to those seen in systems with entirely different molecular components, but the results also give important insight into the underlying mechanisms for the hierarchical assembly of discrete structures in crowded environments. Cells, for instance, have a macromolecular content of up to 40% [20], which is more than a factor of two above the maximum threshold used in this study. Clearly this is a physical factor that must be considered in the assembly of well-defined cellular structures from mechanically dissimilar, filamentous, biopolymer components such as actin, microtubules, vimentin and keratin. Additionally, the broad interest in applying DNA-based macromolecules, often those of an extended rod-like geometry and in the size regime subject to crowding effects [16, 45–48], as intracellular therapeutics, suggests that this basic assembly mechanism should be considered.

Acknowledgments

We like to thank Bernd Kohlstrunk for his support in constructing the custom-build thermocycler and Carsten Schuldt for his help with graphic representations. Further, we thank Tom Golde, Tina Händler, Paul Heine, Jessica Lorenz, Christin Möser, and Carsten Schuldt for helpful discussions and proof reading the manuscript. MG and JS acknowledge the support by the graduate school 'Building with Molecules and Nano-Objects' (BuildMoNa—GSC 185/1) and the DFG Forschergruppe (FOR 877). Part of this work has been supported through the Fraunhofer Attract Project (601683) and the German Science Foundation (DFG—KA 1116/14-1).

Appendix

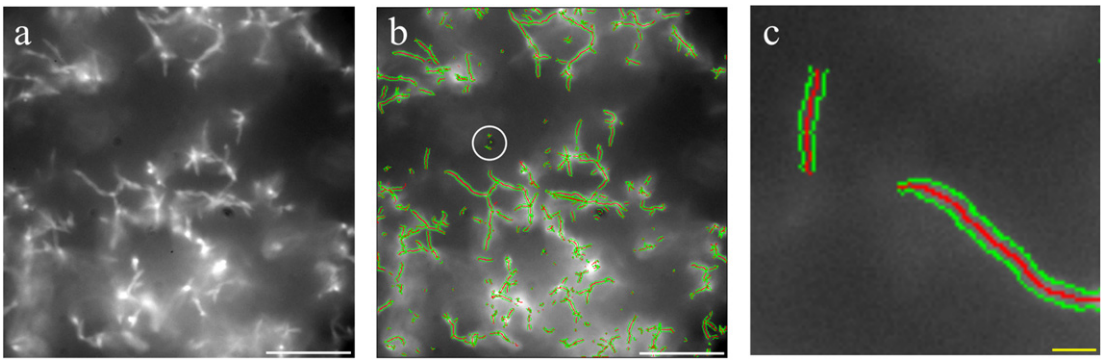

Figure A1. Ridge detection algorithm used to determine bundle width. (a) Gray scale image of 6HT at 16 μM DNA concentration and 5% PEG content. (b) Analysis of the gray scale image yields the backbone (red) and the determined width (green) of the bundle. The white scale bar is 20 μm. (c) Zoomed image of a tracked bundle. The yellow scale bar is 2 μm.

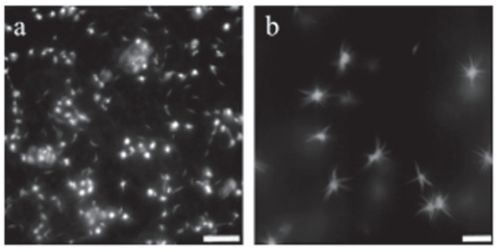

Figure A2. 4HT at 16 μM DNA concentration and 15% PEG content show isolated aster-like structures. (a) Low magnification (133 $\times$ 133 μm). (b) High magnification (83 $\times$ 83 μm). The left scale bar is 20 μm, the right scale bar 10 μm.

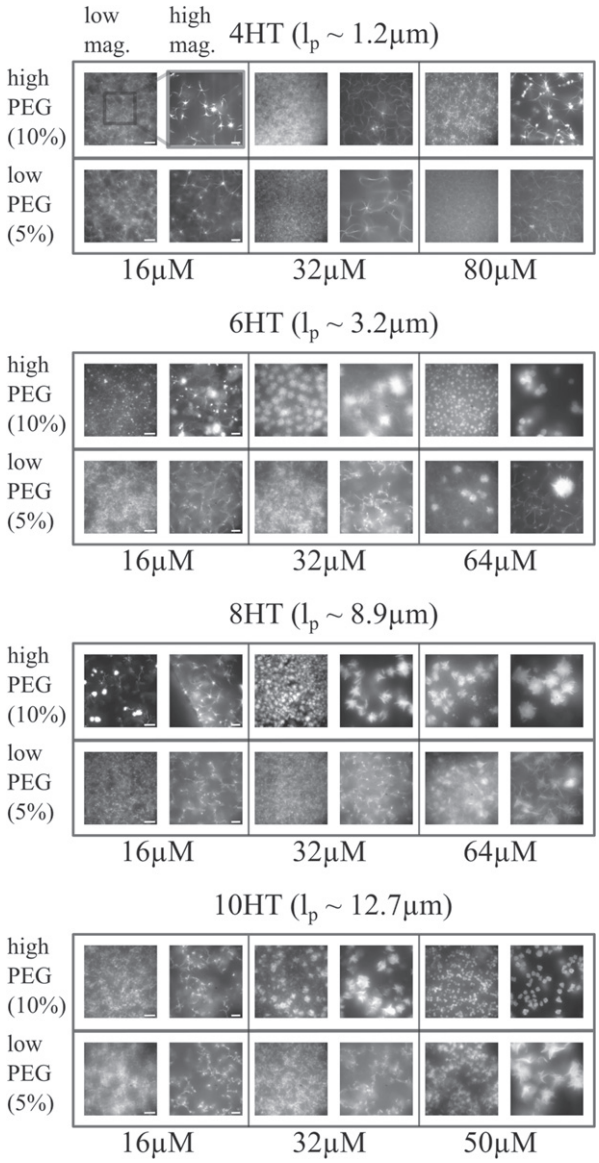

Figure A3. Observed structures for all investigated DNA nanotubes for low (5%) and high (10%) PEG content. The concentration below represents the concentration of each oligo and thus of nanotube unit-rings. Within each box, the left picture represents a low magnification (133 × 133 μm) and the right picture a high magnification (83 × 83 μm). The left scale bar is 20 μm and the right scale bar in the zoomed inset is 10 μm.

Table A1. DNA sequences used for the hybridization of all DNA nanotubes.

Name	Sequence (5′ to 3′)
U1	GGCGATTAGGACGCTAAGCCACCTTTAGATCCTGTATCTGGT
U1-Cy3	Cy3-TTGGCGATTAGGACGCTAAGCCACCTTTAGATCCTGTATCTGGT
U2	GGATCTAAAGGACCAGATACACCACTCTTCCTGACATCTTGT
$U2_{alt}$	CTATGATCTTTGGATCTAAAGGACCAGATACACCACTCTTCCTGACATCTTGT
U3	GGAAGAGTGGACAAGATGTCACCGTGAGAACCTGCAATGCGT
$U3_{alt}$	GATCATAGTTTGGAAGAGTGGACAAGATGTCACCGTGAGAACCTGCAATGCGT
U4	GGTTCTCACGGACGCATTGCACCGCACGACCTGTTCGACAGT
U5	GGTCGTGCGGACTGTCGAACACCAACGATGCCTGATAGAAGT
U6	GGCATCGTTGGACTTCTATCAATGCACCTCCAGCTTTGAATG
U7	GGAGGTGCATCATTCAAAGCTAACGGTAACTATGACTTGGGA
U8	TAGTTACCGTTTCCCAAGTCAAACACTAGACACATGCTCCTA
U9	GTCTAGTGTTTAGGAGCATGTCGAGACTACACCCTTGCCACC
T4	GGTTCTCACGGACGCATTGCACCTAATCGCCTGGCTTAGCGT
T6	GGCATCGTTGGACTTCTATCACCTAATCGCCTGGCTTAGCGT
T8	TAGTTACCGTTTCCCAAGTCACCTAATCGCCTGGCTTAGCGT
T10	GTGTAGTCTCGGGTGGCAAGGCCTAATCGCCTGGCTTAGCGT

References

[1] Whitesides G M and Grzybowski B 2002 Self-assembly at all scales *Science* **295** 2418–21
[2] Consta S 2010 Manifestation of rayleigh instability in droplets containing multiply charged macroions *J. Phys. Chem.* B **114** 5263–8
[3] Losensky L, Chiantia S, Holland G, Laue M, Petran A, Liebscher J and Arbuzova A 2014 Self-assembly of a cholesteryl-modified nucleoside into tubular structures from giant unilamellar vesicles *RSC Adv.* **5** 4502–10
[4] Gibaud T *et al* 2012 Reconfigurable self-assembly through chiral control of interfacial tension *Nature* **481** 348–51
[5] Marco C, Gómez M A, Ellis G and Arribas J M 2002 Activity of a β-nucleating agent for isotactic polypropylene and its influence on polymorphic transitions *J. Appl. Polym. Sci.* **86** 531–9
[6] Cross M C and Hohenberg P C 1993 Pattern formation outside of equilibrium *Rev. Mod. Phys.* **65** 851–1112
[7] Backouche F, Haviv L, Groswasser F and Bernheim-Groswasser A 2006 Active gels: dynamics of patterning and self-organization *Phys. Biol.* **3** 264
[8] Huber F, Strehle D, Schnauß J and Käs J 2015 Formation of regularly spaced networks as a general feature of actin bundle condensation by entropic forces *New J. Phys.* **17** 043029
[9] Nédélec F J, Surrey T, Maggs A C and Leibler S 1997 Self-organization of microtubules and motors *Nature* **389** 305–8
[10] Smith D, Ziebert F, Humphrey D, Duggan C, Steinbeck M, Zimmermann W and Käs J 2007 Molecular motor-induced instabilities and cross linkers determine biopolymer organization *Biophys. J.* **93** 4445–52
[11] Piet D L, Straube A V, Snezhko A and Aranson I S 2013 Viscosity control of the dynamic self-assembly in ferromagnetic suspensions *Phys. Rev. Lett.* **110** 198001
[12] Snezhko A and Aranson I S 2011 Magnetic manipulation of self-assembled colloidal asters *Nat. Mater.* **10** 698–703
[13] Huber F, Strehle D and Käs J 2012 Counterion-induced formation of regular actin bundle networks *Soft Matter* **8** 931–6
[14] Konikoff F M, Chung D S, Donovan J M, Small D M and Carey M C 1992 Filamentous, helical, and tubular microstructures during cholesterol crystallization from bile. Evidence that cholesterol does not nucleate classic monohydrate plates *J. Clin. Invest.* **90** 1155–60
[15] Surrey T, Nedelec F, Leibler S and Karsenti E 2001 Physical properties determining self-organization of motors and microtubules *Science* **292** 1167–71
[16] Sellner S, Kocabey S, Nekolla K, Krombach F, Liedl T and Rehberg M 2015 DNA nanotubes as intracellular delivery vehicles in vivo *Biomaterials* **53** 453–63
[17] Halley J D and Winkler D A 2008 Classification of emergence and its relation to self-organization *Complexity* **13** 10–5
[18] Huber F, Schnauß J, Rönicke S, Rauch P, Müller K, Fütterer C and Käs J 2013 Emergent complexity of the cytoskeleton: from single filaments to tissue *Adv. Phys.* **62** 1–112
[19] Asakura S and Oosawa F 1958 Interaction between particles suspended in solutions of macromolecules *J. Polym. Sci.* **33** 183–92
[20] Ellis R J 2001 Macromolecular crowding: an important but neglected aspect of the intracellular environment *Curr. Opin. Struct. Biol.* **11** 114–9
[21] Hilitski F, Ward A R, Cajamarca L, Hagan M F, Grason G M and Dogic Z 2015 Measuring cohesion between macromolecular filaments one pair at a time: depletion-induced microtubule bundling *Phys. Rev. Lett.* **114** 138102
[22] Hosek M and Tang J X 2004 Polymer-induced bundling of F actin and the depletion force *Phys. Rev.* E **69** 051907
[23] Schnauß J, Golde T, Schuldt C, Schmidt B U S, Glaser M, Strehle D, Händler T, Heussinger C and Käs J A 2016 Transition from a linear to a harmonic potential in collective dynamics of a multifilament actin bundle *Phys. Rev. Lett.* **116** 108102
[24] Strehle D, Schnauß J, Heussinger C, Alvarado J, Bathe M, Käs J and Gentry B 2011 Transiently crosslinked F-actin bundles *Eur. Biophys. J.* **40** 93–101
[25] Suzuki A, Yamazaki M and Ito T 1996 Polymorphism of F-actin assembly: I. A quantitative phase diagram of F-actin *Biochemistry* (*Mosc.*) **35** 5238–44
[26] Kouwer P H J *et al* 2013 Responsive biomimetic networks from polyisocyanopeptide hydrogels *Nature* **493** 651–5
[27] Okoshi K, Nagai K, Kajitani T, Sakurai S and Yashima E 2008 Anomalous stiff backbones of helical poly (phenyl isocyanide) derivatives *Macromolecules* **41** 7752–4
[28] Wollman A J M, Sanchez-Cano C, Carstairs H M J, Cross R A and Turberfield A J 2014 Transport and self-organization across different length scales powered by motor proteins and programmed by DNA *Nat. Nanotechnol.* **9** 44–7
[29] Schiffels D, Liedl T and Fygenson D K 2013 Nanoscale structure and microscale stiffness of DNA nanotubes *ACS Nano* **7** 6700–10
[30] Yin P, Hariadi R F, Sahu S, Choi, Harry M T, Park S H, Labean T H and Reif J H 2008 Programming DNA tube circumferences *Science* **321** 824–6
[31] Hariadi R F, Yurke B and Winfree E 2015 Thermodynamics and kinetics of DNA nanotube polymerization from single-filament measurements *Chem. Sci.* **6** 2252–67
[32] Bi S, Dong Y, Jia X, Chen M, Zhong H and Ji B 2015 Self-assembled multifunctional DNA nanospheres for biosensing and drug delivery into specific target cells *Nanoscale* **7** 7361–7
[33] Lee J B *et al* 2012 A mechanical metamaterial made from a DNA hydrogel *Nat. Nanotechnol.* **7** 816–20
[34] Shopsowitz K E, Roh Y H, Deng Z J, Morton S W and Hammond P T 2014 RNAi-microsponges form through self-assembly of the organic and inorganic products of transcription *Small* **10** 1623–33
[35] Yata T, Takahashi Y, Tan M, Hidaka K, Sugiyama H, Endo M, Takakura Y and Nishikawa M 2015 Efficient amplification of self-gelling polypod-like structured DNA by rolling circle amplification and enzymatic digestion *Sci. Rep.* **5** 14979
[36] Zhu G, Hu R, Zhao Z, Chen Z, Zhang X and Tan W 2013 Noncanonical self-assembly of multifunctional dna nanoflowers for biomedical applications *J. Am. Chem. Soc.* **135** 16438–45
[37] Livolant F, Levelut A M, Doucet J and Benoit J P 1989 The highly concentrated liquid-crystalline phase of DNA is columnar hexagonal *Nature* **339** 724–6
[38] Nakata M, Zanchetta G, Chapman B D, Jones C D, Cross J O, Pindak R, Bellini T and Clark N A 2007 End-to-end stacking and liquid crystal Condensation of 6- to 20-base pair dna duplexes *Science* **318** 1276–9
[39] Zanchetta G, Nakata M, Buscaglia M, Bellini T and Clark N A 2008 Phase separation and liquid crystallization of complementary sequences in mixtures of nanoDNA oligomers *Proc. Natl Acad. Sci.* **105** 1111–7
[40] Steger C 1998 An unbiased detector of curvilinear structures *IEEE Trans. Pattern Anal. Mach. Intell.* **20** 113–25
[41] Pérez F and Granger B E 2007 IPython: a system for interactive scientific computing *Comput. Sci. Eng.* **9** 21–9
[42] Wu Z, Wang G, Zhang M, Wang K and Fu Q 2015 Facilely assess the soluble behaviour of the β-nucleating agent by gradient temperature field for the construction of heterogeneous crystalline-frameworks in iPP *Soft Matter* **12** 594–601
[43] Konikoff F M, Chung D S, Donovan J M, Small D M and Carey M C 1992 Filamentous, helical, and tubular microstructures during cholesterol crystallization from bile. Evidence that cholesterol does not nucleate classic monohydrate plates *J. Clin. Invest.* **90** 1155–60

[44] Gentry B, Smith D and Käs J 2009 Buckling-induced zebra stripe patterns in nematic F-actin *Phys. Rev.* E **79** 031916
[45] Jiang Q, Song C, Nangreave J, Liu X, Lin L, Qiu D, Wang Z-G, Zou G, Liang X, Yan H and Ding B 2012 DNA origami as a carrier for circumvention of drug resistance *J. Am. Chem. Soc.* **134** 13396–403
[46] Zhao Y-X, Shaw A, Zeng X, Benson E, Nyström A M and Högberg B 2012 DNA origami delivery system for cancer therapy with tunable release properties *ACS Nano* **6** 8684–91
[47] Ko S, Liu H, Chen Y and Mao C 2008 DNA nanotubes as combinatorial vehicles for cellular delivery *Biomacromolecules* **9** 3039–43
[48] Kocabey S, Meinl H, MacPherson I S, Cassinelli V, Manetto A, Rothenfusser S, Liedl T and Lichtenegger F S 2014 Cellular uptake of tile-assembled DNA nanotubes *Nanomaterials* **5** 47–60